Proceeding Paper

Topography Pre-Treatment of Laser-Textured Surfaces for Friction Simulation in AVL Excite †

Gábor Laki *, László Boros and András Lajos Nagy

Department of Propulsion Technology, Széchenyi István University, Egyetem tér 1, H-9026 Győr, Hungary; boros.laszlo@ga.sze.hu (L.B.); andras.nagy1@sze.hu (A.L.N.)
* Correspondence: laki.gabor@sze.hu
† Presented at the Sustainable Mobility and Transportation Symposium 2024, Győr, Hungary, 14–16 October 2024.

Abstract: This study presents the challenges arising during the numerical design and simulation of surface-microtextured piston rings. The evaluation of performance is based on the values of asperity and hydrodynamic friction, as well as the lubricant film thickness. The simulation tool AVL Excite Piston & Rings is used to perform the calculations. The aim of this study is to understand how selected surface pre-processing (pre-treatment) steps affect the calculations. Two methods are presented to achieve a realistic surface topography representative of a state after running-in. Pre-treatment is performed through metrological filtering and thresholding of the topography, and Gaussian smoothing of the virtually applied micro-texture array is carried out. The results show the anticipated behavior of decreasing asperity and hydrodynamic friction losses with the concurrent application of both techniques.

Keywords: micro-contact analysis; surface texturing; asperity pressure; surface pre-treatment

1. Introduction

With tighter emission standards, the need to reduce harmful exhaust components and carbon dioxide emissions from internal combustion engines (ICEs) is continuously rising. Achieving reduced fuel consumption through lower frictional losses contributes to fulfilling these environmental goals. Studies have demonstrated that laser surface texturing can effectively reduce friction by improving load-carrying capacity, lowering adhesion, decreasing the effective contact area, and collecting wear particles, leading to improved performance [1]. Additionally, laser texturing with optimized parameters, such as laser power, scanning speed, and processing times, has been found to enhance the anti-friction properties of materials like 304 stainless steel, resulting in reduced friction coefficients and wear rates [2]. Furthermore, the use of laser surface texturing has been explored in the context of internal combustion engines to reduce mechanical losses and improve efficiency through enhanced lubrication and reduced friction in sliding and rolling contacts [3].

Various studies have focused on simulating the effects of laser surface texturing on different materials. In a study by Mandal et al. [4] a 2D FEM model was developed to predict temperature and velocity fields during the surface texturing of IN718 powder, showing a decrease in micro-convex dimple height with more pulses. Another study by Heinrich et al. [5] utilized 3D computational fluid dynamics models to simulate the formation of resolidified surface structures through laser interference patterning, matching experimental data in terms of shape and dimensions, providing insights into the process parameters' impacts. Laser ablation for fiber surface modification was also investigated with a 3D model analyzing the thermal mechanism and surface topography evolution during pulsed CO_2 laser ablation, showing stable ablation depth after the second pulse [6]. Additionally, a study on the wettability of laser-ablated microstructures highlighted the influence of groove parameters on contact angle, with a CFD analysis aiding in defining the optimal surface structures for desired wettability [7].

Advanced simulations have been conducted utilizing AVL Excite Power Unit to analyze the frictional behavior in internal combustion engines under varying load and speed conditions. Zabala et al. demonstrated, through a simulation, that diamond-like carbon (DLC) coatings combined with low-viscosity 5W-30 lubricants yielded minimal friction in the evaluated scenarios [8]. Michelberger et al. used AVL Excite to verify and enhance the data collection of a self-developed long-stroke tribometer for high-definition friction measurements [9]. Tomanik et al. used AVL Excite Piston & Rings to compare cylinder bore finishes and oil types to reduce friction. The simulation successfully predicted that a plateau-honed finish performs better than a mirror finish [10]. EHD simulation in AVL Excite Piston & Rings showed that microchannels manufactured through the laser ablation of an ICE compression ring's contact surface contributes to lower friction losses, where the channels increased hydrodynamic pressure in certain operating conditions [11].

This paper delineates the methodological framework for setting up engine simulations aimed at elucidating the frictional characteristics of top piston rings featuring laser-induced micro-dimples on their running faces. The aim of the present study is to determine the key influencing factors during the preparation of input datasets, specifically how the effect of running-in is reflected in the simulation.

2. Materials and Methods

AVL Excite Piston & Rings 2023 was used to assess the influence of microtextured surfaces on the tribology of piston rings. The software's micro-contact analysis module allows the use of 3D surface topographies acquired through classical or optical metrology for calculating both the asperity contact properties (acc. to Greenwood and Tripp [12]), and flow factors (based on Patir and Cheng [13]). Flow factors were considered during solving the Reynolds equation to determine the hydrodynamic pressure, film thickness and hydrodynamic friction. The asperity contact pressure was used to calculate asperity friction. Real cylinder bore surfaces and corresponding GDC coated piston ring samples were digitalized on a Leica DCM3D Confocal Microscope and included in the micro-contact analysis simulations as contact pairs. Ring dynamics calculations were run using the simplified 3D Ring model. In order to reduce the influence of local abnormalities on the actual surfaces, the topology was recorded in multiple locations along the physical samples. Various microscopic dimple configurations were engineered using MATLAB and superimposed onto the digitized piston ring surfaces.

Two key steps were identified during the preparation of virtual micro-dimpled surfaces. To investigate the effect of these factors, a selection of preparatory simulations were conducted. The identified challenges are as follows:

- As-manufactured surfaces exhibit protruding asperities and sharp edges, which are generally removed during running-in; hence, a topography scan of a "virgin" surface is not representative in a simulation, where wear is not considered explicitly.
- The virtual dimple preparation leaves a sharp transition at the edge of the dimples, which will induce increased asperity contact pressures.

2.1. Virtual Running-In

A digital filtering routine in MountainsMAP v8 was investigated to simulate surface topography after running-in. Surfaces were first leveled and flattened to remove any inclination and form. An order 0 robust Gaussian metrological filter with an 8 μm cut-off was applied to remove ultra-fine surface features and measurement noise. A material ratio-based thresholding filter was applied that excluded points corresponding to the lower 10% region of the material ratio curve, resulting in the removal of protruding regions. Finally, a morphological opening and closing filter with a 35 μm spherical structuring element was applied to smooth out the edges of asperities. Figure 1. shows an example of the surface topography before and after applying the digital filtering routine.
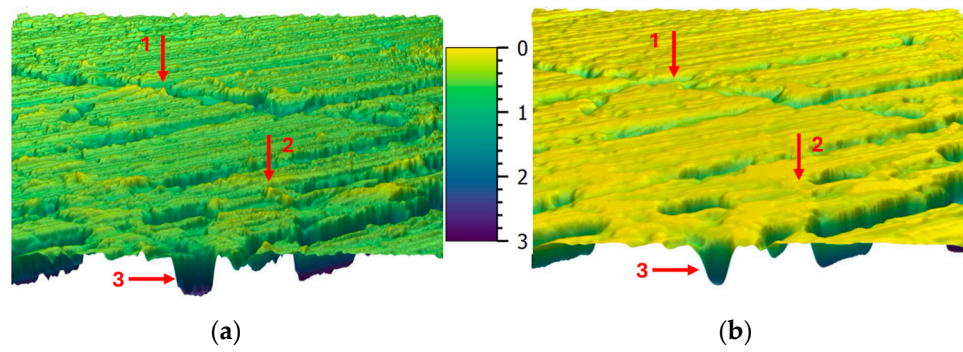
(**a**)   (**b**)

Figure 1. Exemplary surface scan of cylinder's running surface showing (**a**) topography before digital filtering (virtual running-in) and (**b**) topography after digital filtering. Red arrows highlight surface features, which were smoothed during virtual running-in: protruding asperities (1,2) are removed, while valleys (3) are rounded, which resembles naturally occurring phenomena due to wear (1,2) and accumulation of wear debris (3).

2.2. Gaussian Smoothing

A sharp transition is produced between the original surface topology and the dimples due to the nature of how micro-dimples are applied to the piston ring surface scans to create the desired micro-dimple surface. A large dimple array is patched first, which has its reference plateau at Z = 0, with the desired dimples protruding in the negative Z direction. This dimple array is cropped to the desired size (identical to the surface scans) and the dimple array is subtracted from the surface scan. The resulting sharp transition at the edge of the dimples can lead to computational inaccuracies in the simulations. To address this issue and approximate a more realistic dimple geometry, a Gaussian smoothing operation is applied to the dimple array before subtracting it from the surface scan. Figure 2 depicts a schematic cross-section profile of a dimple with and without Gaussian smoothing, showcasing the transition at the edge of the dimple, as well as the resulting change in the dimple geometry and overall contact area. An average contact area reduction of 10% after Gaussian smoothing is established with various dimple sizes. The filtering results in a change in the textured area. The average increase in the textured area with Gaussian smoothing is found to be 17%.
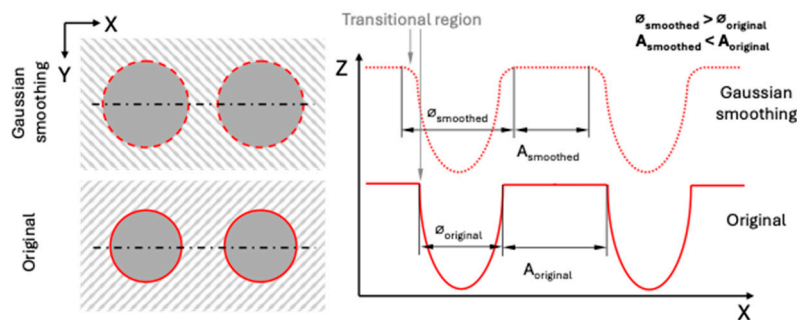

Figure 2. A visual description of the effect of Gaussian smoothing, showing a stylized dimpled surface from a topside view and in a cross-section profile. As the transitional region between the plateau (hatched) and the dimple (dark gray) is rounded during smoothing, the dimple diameter increases ($\varnothing_{smoothed} > \varnothing_{original}$) and the total plateau area decreases ($A_{smoothed} < A_{original}$).

2.3. Simulation Setup

The effect of the number of topology combinations on the micro-contact analysis results is also investigated by comparing two runs, one including a total of 9 piston ring and cylinder surface scan pairs and one including a total of 27 piston ring and cylinder surface scan pairs.

Running the micro-contact analysis yields a collection of intermediary results detailing the effect of surface microtopography on both hydrodynamic and asperity friction. These intermediary results include asperity contact pressures, which are used during the development of the pre-processing workflow to evaluate cropping and smoothing. In addition to the micro-contact results, full-scale Piston & Rings cycle simulations are run using a tutorial model of a 1.4 L petrol engine. The lubricant properties are determined by the built-in SAE 0-W20 engine oil model. Calculations are performed at engine speeds of 1250 rpm, 1500 rpm and 1750 rpm. Three key lubrication indicators are chosen from the results to evaluate the effect of the presented pre-processing techniques. These indicators are the mean asperity friction power loss, mean hydrodynamic friction power loss, and minimum oil film thickness, all evaluated on the running face of the top piston ring.

3. Results and Discussion

Using a total of 9 contact pairs ensures a reasonable simulation runtime, whereas increasing the number of contact pairs to 27 leads to a linear increase in runtime, but only marginal variation in the intermediary results. As the upcoming steps of research include the analysis and comparison of numerous dimple configurations, an economical solution is sought for the ranking phase; hence, only nine contact pairs are considered. In the later stages, the best performing configurations can be simulated using a higher number of surface scans, to ensure better accuracy.

3.1. Micro-Contact Analysis Results

The analysis results with and without digital filtering and Gaussian smoothing depicted on Figure 3 show the effect of topography preparation on the tendencies of mean asperity contact pressure (p_{Asp} [MPa]). The presented values are given as a function of the ratio of the separation distance between the two contacting surfaces (h [μm]) to the standard deviation of the surface roughness (σ [μm]). This ratio is denoted by H [-]; $H = 1$ represents a condition, where the separation distance (the nominal distance between the arithmetic mean plane of the rough surfaces) is equal to the standard deviation of the surface roughness.
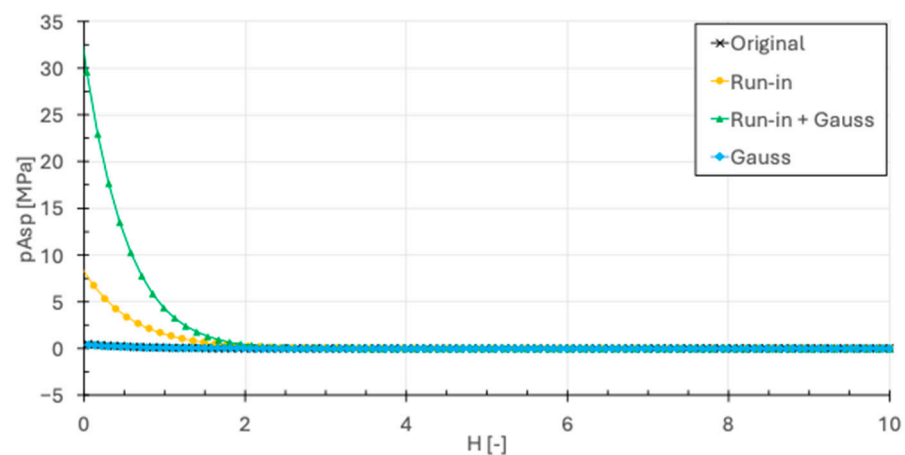

Figure 3. The mean asperity contact pressure (p_{Asp}) as a function of the ratio of the separation distance between the two contacting surfaces to the standard deviation of the surface roughness (H).

The scanned and virtually textured (original) surfaces show a very shallow curve, which can be attributed to the surfaces having local protruding asperities. These exhibit elevated contact pressure, but due to their localized nature and discrete number, contribute little to the mean asperity contact pressure. Since Gaussian smoothing only affects the edges of dimples, the effect of this procedure alone is negligible. Applying digital filtering (virtual running-in) has a pronounced effect on mean asperity contact pressure, as this process removes local asperity peaks and significantly flattens the surfaces, resulting in a

smoother contact surface. As H decreases, the flattened surfaces form a larger real contact area, which contributes to a rising p_{Asp} value. Using both filtering and Gaussian smoothing results in an even faster rise in p_{Asp} with decreasing H. This is theorized to be a result of the reduction in the overall real contact area, as Gaussian smoothing rounds the edges of dimples, which is depicted in Figure 2. Reducing the real contact area of the virtually run-in, flattened surface results in higher contact pressure at the same nominal separation. As these findings agree with basic physical phenomena, i.e., decreasing the number of outlier asperities and decreasing the real contact area leads to an increase in mean asperity contact pressure, the procedure including both virtual running-in (digital filtering) and Gaussian smoothing will be utilized for further investigations.

3.2. Full-Cycle Simulation Results

The full-cycle calculation results are presented for mean asperity friction power loss (mAFP), mean hydrodynamic friction power loss (mHFP), and mean of minimum oil film thickness (mMOFT) in Figure 4. The values are represented as percentage changes related to a calculation where none of the discussed topography pre-treatment methods were utilized. A noticeable change can be seen in mAFP and mHFP with the application of virtual running-in, which results in a significant drop in total friction power loss. This phenomenon can be attributed to a flatter overall surface topography, resulting in a smoother running surface. On the other hand, there is a far less significant change in oil film thickness, as the general oil retention capacity of the surface was not directly affected by the applied methods. The presented results are in accordance with general expectations based on the underlying physical processes of real-life running-in, which results in the removal of protruding asperities, therefore flattening the topography and creating a continuous running surface. Interestingly, only applying the step of Gaussian smoothing of the dimple arrays negatively affects asperity friction power losses. The exact understanding of this phenomenon requires further research, which lies outside the scope of this article.
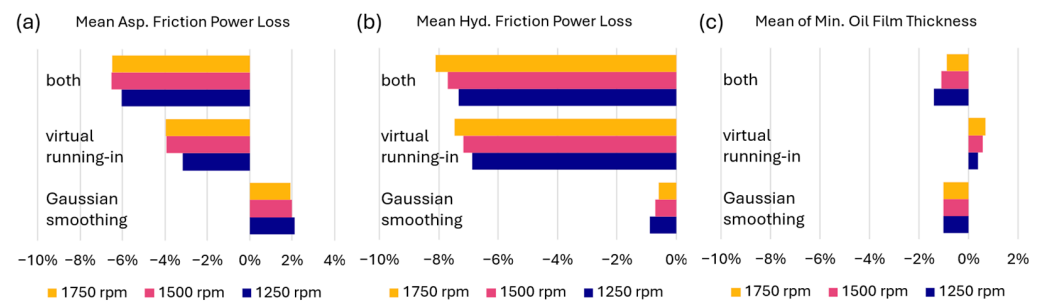

Figure 4. Results of (**a**) mean asperity friction power loss, (**b**) mean hydrodynamic friction power loss, and (**c**) mean of minimum oil film thickness calculated on running face of top piston ring, represented as percentage change in mean value during one full cycle of 720 °C compared to calculation without pre-treatment.

4. Conclusions

Applying certain pre-processing steps is an integral part of simulation, yet the exact steps tend to vary from method to method and application to application. This study investigated the effect of a digital filtering (virtual running-in) and a Gaussian edge smoothing step in the pre-treatment workflow of scanned and digitally textured surface microslides used for friction loss calculations. In order to assess the effect of virtual running-in and edge smoothing, surface scans were taken from series production engine parts and subjected to a series of filtering steps in MountainsMAP, and then were virtually applied an array of micro-dimples, with smoothed edges. The two pre-treatment methods were investigated separately as well and compared to the simulation results without applying a pre-treatment. The following conclusion can be drawn:

- Applying no pre-treatment results in unrealistically low asperity contact pressure at a nominal separation-to-roughness ratio of 0, due to a high number of protruding asperities;
- Virtual running-in results in an anticipated decline in both asperity and hydrodynamic friction power loss;
- Gaussian smoothing of the dimple edges results in unexpected behavior, which needs further experimentation to explain.

Author Contributions: Conceptualization, A.L.N. and G.L.; software, G.L. and L.B.; investigation, G.L.; writing—original draft preparation, G.L.; writing—review and editing, G.L. and A.L.N.; visualization, G.L. and L.B.; and A.L.N. All authors have read and agreed to the published version of the manuscript.

Institutional Review Board Statement: Not applicable.

Informed Consent Statement: Not applicable.

Data Availability Statement: Data for this study are not publicly available.

Conflicts of Interest: The authors declare no conflicts of interest. The funders had no role in the design of the study; in the collection, analyses, or interpretation of the data; in the writing of the manuscript; or in the decision to publish the results.

References

1. Roushan, A.; Chetan. Influence of laser parameters on the machining performance of textured cutting tools. *Opt. Laser Technol.* **2022**, *165*, 109569. [CrossRef]
2. Li, X.; Li, G.; Lei, Y.; Gao, L.; Zhang, L.; Yang, K. Influence of Laser Surface Texture on the Anti-Friction Properties of 304 Stainless Steel. *Machines* **2023**, *11*, 473. [CrossRef]
3. Laki, G.; Nagy, A.L.; Rohde-Brandenburger, J.; Hanula, B. A Review on Friction Reduction by Laser Textured Surfaces. *Tribol. Online* **2022**, *17*, 318–334. [CrossRef]
4. Mandal, V.; Tiwari, V.; Sarkar, M.; Singh, S.S.; Ramkumar, J. Numerical and experimental study of micro-convex dimple developed by laser additive manufacturing for surface applications. *Manuf. Technol. Today* **2023**, *22*, 45–50. [CrossRef]
5. Heinrich, M.; Voisiat, B.; Lasagni, A.F.; Schwarze, R. Numerical simulation of periodic surface structures created by direct laser interference patterning. *PLoS ONE* **2023**, *18*, e0282266. [CrossRef] [PubMed]
6. Hu, C.; Wu, H.; Ma, X. Numerical simulation of surface topography evolution during pulsed CO_2 laser ablation of fiber. In Proceedings of the Sixth International Symposium on Laser Interaction with Matter (SPIE), Ningbo, China, 10–13 August 2022; Volume 12459, p. 1245902. [CrossRef]
7. Novosád, J.; Dvořák, L.; Peukert, P. CFD simulation of wettability of laser-structured surfaces. In *EPJ Web of Conferences*; EDP Sciences: Les Ulis, France, 2022; Volume 269. [CrossRef]
8. Zabala, B.; Igartua, A.; Fernández, X.; Priestner, C.; Ofner, H.; Knaus, O.; Nevshupa, R. Friction and wear of a piston ring/cylinder liner at the top dead centre: Experimental study and modelling. *Tribol. Int.* **2017**, *106*, 23–33. [CrossRef]
9. Michelberger, B.; Jaitner, D.; Hagel, A.; Striemann, P.; Kröger, B.; Leson, A.; Lasagni, A.F. Combined measurement and simulation of piston ring cylinder liner contacts with a reciprocating long-stroke tribometer. *Tribol. Int.* **2021**, *163*, 107146. [CrossRef]
10. Tomanik, E.; Profito, F.; Sheets, B.; Souza, R. Combined lubricant–surface system approach for potential passenger car CO_2 reduction on piston-ring-cylinder bore assembly. *Tribol. Int.* **2020**, *149*, 105514. [CrossRef]
11. Michelberger, B.; Schell, F.; Jaitner, D.; Götze, A.; Leupolt, B.; Wetzel, F.J.; Lasagni, A.F. Positive Effect of Periodic Micropatterns on Compression Ring Friction. *Adv. Eng. Mater.* **2023**, *25*, 2201708. [CrossRef]
12. Greenwood, J.A.; Tripp, J.H. The Contact of Two Nominally Flat Rough Surfaces Arch. *Proc. Inst. Mech. Eng.* **1970**, *185*, 625–634. [CrossRef]
13. Patir, N.; Cheng, H.S. Application of Average Flow Model to Lubrication Between Rough Sliding Surfaces. *J. Lubr. Technol.* **1979**, *101*, 220–229. [CrossRef]